Microstructural consequences of nanosilica addition on aerial lime binding materials: influence of different drying conditions

J.I. Alvarez[a,*], J.M. Fernández[b], I. Navarro-Blasco[c], A. Duran[d], R. Sirera[e]

[a] José Ignacio Álvarez, Inorganic Materials & Environment (MIMED), Department of Chemistry and Soil Sciences, School of Sciences, University of Navarra, c/ Irunlarrea, 1, 31008 Pamplona, Spain, Phone: +34 948 425600, Fax: +34 948 425740 jalvarez@unav.es, mimed@unav.es

[b] José María Fernández, Inorganic Materials & Environment (MIMED), Department of Chemistry and Soil Sciences, School of Sciences, University of Navarra, c/ Irunlarrea, 1, 31008 Pamplona, Spain, Phone: +34 948 425600, Fax: +34 948 425740 jmfdez@unav.es

[c] Íñigo Navarro-Blasco, Inorganic Materials & Environment (MIMED), Department of Chemistry and Soil Sciences, School of Sciences, University of Navarra, c/ Irunlarrea, 1, 31008 Pamplona, Spain, Phone: +34 948 425600, Fax: +34 948 425740, inavarro@unav.es

[d] Adrián Durán, Inorganic Materials & Environment (MIMED), Department of Chemistry and Soil Sciences, School of Sciences, University of Navarra, c/ Irunlarrea, 1, 31008 Pamplona, Spain, Phone: +34 948 425600, Fax: +34 948 425740, adrianduran@unav.es

[e] Rafael Sirera, Inorganic Materials & Environment (MIMED), Department of Chemistry and Soil Sciences, School of Sciences, University of Navarra, c/ Irunlarrea, 1, 31008 Pamplona, Spain, Phone: +34 948 425600, Fax: +34 948 425740, rsirera@unav.es

ABSTRACT:

The addition of a pozzolanic nanosized material, nanosilica (NS), onto lime binding materials was carried out with the aim of assessing the microstructural modifications attained by its presence that were related to the mechanical behavior. Simultaneously, a comparative study between five different drying methods for water removal was reported, and their influence on the pore structure evaluation

is discussed. Solvent-exchange with isopropanol and freeze-drying methods were shown to remove the excess of free water efficiently, allowing us to measure the gel pores (< 10 nm) of the calcium silicate hydrated (C-S-H) phases and yielding the largest surface area values. By using vacuum drying, oven drying at 60ºC or oven drying at 105ºC macro-, meso- and micropores could not be properly measured. On the other hand, the addition of NS dramatically altered the mesopore range. As a result of the intercalation of NS particles between lime particles, a drop in the population of large and medium capillary pores (in the range of 20-100 nm) was observed, leading to reduced overall porosity. The NS was clearly proven to act as nanofiller. Finally, this filling effect of NS together with the development of C-S-H gel, as a consequence of the pozzolanic-type reaction proved by the increase of population in the micropore range, notably enhanced the compressive strength of the lime binding materials, yielding values more than twice those of the NS-free materials.

*Corresponding Author:

Dr. José I. Alvarez Galindo

Materiales Inorgánicos y Medio Ambiente (MIMED), Dpto. de Química y Edafología, Fac. de Ciencias

Universidad de Navarra, C/ Irunlarrea, 1, 31008 Pamplona (Navarra), Spain

Phone: +34 948 425600 Fax: +34 948 425740

E-mail: jalvarez@unav.es, mimed@unav.es

Keywords: Nanosilica; SEM; pore size distribution; TEM; mesopore; compressive strength

1. Introduction

The relevance of aerial lime-based binding matrices is evidenced by the large variety of studies devoted to them, the number of which has dramatically increased of late [1-4]. The practical applications of these materials range from restoration of cultural heritage to their use in new constructions such as monocouche rendering mortars, coating mortars, etc. Studies have been

published on newly designed and prepared aerial lime binders, in which their mechanical performance and durability, the effect of various aggregates and even the behavior and effectiveness of various admixtures have been analyzed [5-12]. The literature has shown an interest in the incorporation of materials with pozzolanic activity, such as metakaolin [9,13-19], in aerial lime matrices, in order to overcome some of the drawbacks of this kind of binding materials, specially those related to their low mechanical strengths [6,7,20].

Although nanometer-sized silica has been extensively studied in cement-based systems [21-27], our research group has recently investigated the role of nanosilica (NS) incorporation in aerial lime binders [28]. It has been reported that colloidal silica points to small particles consisting of an amorphous SiO_2 core with a hydroxylated surface, which are insoluble in water [24,26]. The size of the particles can be varied between 1 and 500 nm. In cementitious materials, the performance enhancing properties of NS are thought to be achieved through two mechanisms: a filling action and/or a chemical reaction resulting in C-S-H formation. The filling action lies in the fact that the fine particles of NS could be able to fill the meso- and micropores between the cement particles, thereby improving "packing" and thus giving rise to densification of the binding matrix. The chemical reaction between the nanosilica and the $Ca(OH)_2$ to form a gel of calcium silicate hydrate phases (C-S-H, whose pore sizes fall within the micro- and mesopore range [29]) also leads to a mechanical improvement over the curing process [24,26,27]. The assessment of the pore structure, and specific surface area in aerial lime matrices with pozzolanic additions is extremely important in order to fully understand the mechanical behavior and thus the applicability of the resulting materials. This paper aims to perform a thorough examination of the pore size distribution and specific surface area of lime binders modified by the addition of a nanosized material, nanosilica, over time (7, 28 and 91 curing days). Its role as nanofiller is also dealt with in the light of the

79 microstructural modifications caused by its presence. The compressive strength behavior of the
80 samples is related to the micro and mesoporous modifications.
81
82 However, the reliable evaluation of pore sizes, specially in the micro- and mesoporous region,
83 demands almost complete removal of the water [30]. Insufficient drying can lead to distort the
84 measured porosity and porosimetry values, since the pores may become either fully or partially
85 occluded by water. Furthermore, the presence of the remaining water forces carbonation to continue,
86 since atmospheric CO_2 can dissolve into the condensed water inside the pores and react there with
87 part of the dissolved calcium hydroxide to form calcium carbonate, which is ultimately responsible
88 for the hardening of the lime mortar [31,32]. In the presence of pozzolanic additions, the water
89 excess can lead to progressive hydration of calcium silicates formed after the chemical reaction
90 between the lime and the pozzolanic reactive material. In those studies in which the evolution of the
91 porous structure develops as a function of the curing time, the effective removal of excess water is
92 important to ensure the actual correspondence of the porous structure measurements with the curing
93 time.
94
95 In cement matrices, water removal in order to arrest ongoing hydration of the anhydrous phases, and
96 thus obtain reliable measurements of the porous structure, is of the utmost importance and has
97 recently been studied by Zhang and Scherer [33]. A quasi-complete removal of water prior to studies
98 of the porous structure is considered mandatory in cement media, and various methods have been
99 proposed such as use of the dipping process in organic solvent to exchange the water present in the
100 pores and subsequent evaporation of the solvent, the freezing of the sample and subsequent
101 sublimation of the water (i.e. freeze-drying) [34,35], vacuum drying and also oven drying at
102 temperatures ranging between 50º and 105° C. Galle's work [36] points out that these methods have
103 often been used without a clear understanding of how they can affect the microstructure of the

material. Changes in water content may cause microcracks in cement pastes, collapse of small pores, mineralogical and capillary porosity changes, and so on.

Both temperature and time exert a major influence on oven and/or vacuum drying procedures: insufficient drying can lead to incomplete removal of water, while excessive drying can result in collapse of pores and even the occurrence of shrinkage cracks [30,37]. Zhang and Scherer [33] report that in addition to the damage caused by capillary pressure, the different thermal expansion between the aggregates and the binding matrix may also give rise to microcracking. Freeze-drying, by immersion of the sample in liquid N_2 at -196 ° C, produces microcrystals of ice, which may cause stresses in the areas of small pores, even with shrinkage of the finest porosity [36]. Recourse to an organic solvent may lead to a microstructure alteration caused by the reaction of some solvents with the binding compounds (in the case of cement, with the hydration products) [34].

The influence of these various methods employed for water removal prior to the study of the porous structure and of the specific surface area has not been discussed so far in nanosilica-lime and plain lime binding matrices. It must be considered that both the composition and microstructural characteristics of lime mortars are very different from those of the cement mortars [20,38,39]. Therefore, as well as examining the pore structure and specific surface area of nanosilica-modified lime binders, another objective of this work is to perform in these materials a comparative examination of the effect of five different methods of drying on the assessment of the above mentioned microstructural characteristics. The assayed drying methods were: exchange with an organic solvent (isopropanol), freeze-drying, vacuum drying and oven drying at both 60 °C and 105 °C, all of which were also applied over three periods of curing (7, 28 and 91 days).

1.1. Background concerning the pore structure of lime binders

According to many previous studies and in accord with the IUPAC classification for pore size (micropores: < 2 nm; mesopores: 2-50 nm; macropores: > 50 nm) [40], aerial lime-based binders show some macropores that clearly exceed 50 nm [20,30]. Pores larger than 50 μm in diameter appear due to the presence of air-entraining admixtures, entrapped air during the mixing process or an unsuitable degree of mortar compactness. Shrinkage resulting in crack formation could also be responsible for the appearance of large pores. On the other hand, capillary porosity is also formed in the binding matrix and in the interfacial transition zone (ITZ) between the binding matrix and the aggregate particles. Capillary pores occur as a result of the setting and/or of the removal of the mixing water excess [30]. According to Pipilikaki and Beazi-Katsioti [40], large capillaries are pores sized over 50 nm, medium capillaries are pores between 10-50 nm and, finally, small (gel) capillaries are pores ranging from 2.5 nm to 10 nm. Large and medium capillary porosity is closely related to the water/lime and lime/aggregate ratios, and it undergoes changes over time owing to the phenomena of dehydration and carbonation. In quantitative terms, this type of porosity is the most relevant in a lime mortar and has a significant influence on transport processes as well as on the permeability through the structure of the mortar.

In lime mortars, the occurrence of small gel pores can also be observed. These pores (< 10 nm) are due to the porosity of C-S-H phases [29,41]. C-S-H compounds arise as a result of a pozzolanic-type reaction between the lime and reactive siliceous compounds from: i) the aggregate; ii) the lime itself (as in the case of natural hydraulic limes); or iii) the presence of pozzolanic additions (such as metakaolin or nanosilica). It must be emphasized that these small pore size phases can be particularly sensitive to the drying procedures, so the present study focuses on the changes that these drying methods together with the presence of NS cause in these pores.

2. Material and methods

2.1. Materials

Mortars were prepared from slaked aerial lime (Class CL 90-S, according to the previously reported European norm EN 459-1:2011 [20], supplied by CALINSA) as binding material. The aggregate was a standard siliceous sand (99% of SiO_2 in mass), evenly graded, of controlled granulometry, with particle diameter ranging from 0.05 to 2 mm. It was supplied by the Instituto Eduardo Torroja. The nanosilica used was a colloidal suspension of silica with pH = 9.68 and a solid / liquid ratio of 0.28, as supplied by the manufacturer (Ulmen Europa SL). Spherical particles of NS were measured to range between ca. 20 to 150 nm, as proved by TEM examinations (LIBRA 120 energy-filtering TEM (Zeiss) operated at 80 kV) and depicted in Fig. 1.

2.2. Sample preparation and experimental tests

The binding mortar specimens were prepared in 1:1 lime:aggregate ratio by volume, whose corresponding weight ratio was 18.5 wt. % lime and 81.5 wt. % sand (1:3 weight/weight ratio). This ratio was extensively used in previous works on lime mortars and has been reported to be suitable for this kind of materials [4,6,7,20]. Three batches of samples were prepared: a control group of plain lime mortars, MS1 samples, made of just aerial lime and siliceous aggregate, using 28 wt. % of mixing water with respect to the total components of the dry mortar; MS2 samples, with a 3 wt. % added nanosilica with respect to the lime and 28 wt.% of mixing water; and finally the batch MS3, with a 3 wt. % added NS but with 30 wt. % of mixing water. The amount of water was optimized for MS1 samples in order to obtain a suitable mortar consistency. The workability of the mortars was considered optimal when the spread in the flow table test was maintained in the range of 175 ± 5

mm, which was reached with 28 wt.% of mixing water. The mixing water was kept identical for the preparation of samples MS2, in which NS was added. However, the presence of a small particle size material, such as NS, reduces the fluidity of the mixture, increasing the water demand to keep the spread within the 175 ± 5 mm value; for this reason, 30 wt. % mixing water was used in the MS3 batch.

Lime and aggregate were blended for 5 min in a BL-8-CA (Lleal S.A.) solid mixer. Afterwards, the required amount of mixing water –and, where indicated, the NS suspension- was added and mixed for 90 s at low speed in a ETI 26.0072 Proeti mixer. Cylindrical (5 cm height and 3.5 cm diameter) PVC molds were filled with the fresh mixture and were compacted in an automatic compactor for 60 s. Then, they were stored under controlled conditions at 60% relative humidity (RH) and 20 °C. Specimens were demoulded 5 days later. The tests were carried out after curing periods of 7, 28 and 91 days. Three specimens were assayed for every composition (MS1, MS2 and MS3 batches), each selected curing period and all the five drying procedures employed, so that statistical significance and reproducibility of results were ensured.

Specifically, hardened specimens were subjected to five water removal procedures:

1. Solvent exchange: immersion in isopropanol for 7 days and subsequent drying in an oven for 2 days at 60 °C. This solvent was chosen as a consequence of the very low solubility shown for portlandite.
2. Freeze-drying: Immersion of the specimen in liquid N_2 for 5 min, and subsequent sublimation at -40 °C under 1 Pa vacuum for 24 h.
3. Vacuum drying, 3% RH, 23 °C.
4. Oven drying at 60 °C for 7 days
5. Oven drying at 105 °C for 7 days.

Once the samples had been dried after the use of one of the water removal procedures, they were weighed and the thermal behavior, mechanical strength and pore structure of the materials were examined. Thermal analysis was carried out in a TG-DTA 851^{e} (Mettler Toledo) simultaneous thermal analyzer, in alumina crucibles at a heating rate of 10 °C min^{-1}, from 25 °C to 1000 °C, under constant N_2 flow of 20 mL min^{-1} as purge gas. Calcium hydroxide and calcium carbonate contents were evaluated from weight loss detected in thermogravimetric curve, in which the dehydroxylation of $Ca(OH)_2$ was assumed to have occurred at ca. 450 °C, while the decarbonation of $CaCO_3$ took place at ca. 800 °C [42,43].

The specific surface area of the samples was determined by N_2 adsorption isotherms at 77 K using an ASAP2020 (Micromeritics, USA) instrument. The specific surface area was calculated using the multipoint BET method at relative pressures between 0.03 and 0.22. It has been reported that BET method can properly estimate micropores and gel pores as well as the surface area of medium and small capillary pores [44].

The pore size distribution (PSD) was studied by (i) mercury intrusion porosimetry (MIP) in a Micromeritics AutoPore IV 9500 with a pressure ranging from 0.0015 to 207 MPa. The equipment automatically registers pressure, pore diameter and intrusion volume, and (ii) from the N_2 adsorption isotherms data: the Barret-Joyner-Halenda (BJH) method was chosen to accurately evaluate the distribution of pore size in the mesopore range (adsorption isotherm branch) [45]. The micropore size distribution was calculated using the Hovarth-Kawazoe method for slit pore geometry, which has been reported the most suitable geometry for C-S-H gel pores [29].

Compressive strength tests were determined on a Proeti ETI 26.0052 press at a loading rate of 50 $N \cdot s^{-1}$. For comparison purposes of the mechanical behavior, also two batches of samples with the same composition of MS2 and MS3 samples, except that they were - in this instance- loaded with 6 wt.% NS, and after the different curing periods were subjected to the mechanical tests. Finally, where deemed necessary, the microstructure of the samples was observed in a Hitachi S-4800 (Hitachi, Japan) scanning electron microscope (SEM) coupled with an EDS detector.

3. Results and discussion

3.1 MIP and specific surface area studies

Experimental results for pore size distribution obtained by MIP from the MS1 samples subjected to the solvent exchange with isopropanol showed, after 7 curing days, an average pore size of 0.6 μm (Fig. 2a). This diameter can be defined as the critical diameter and reflects the more abundant interconnected pore size. A certain volume of pores with a larger diameter -between 5 and 20 μm- was also found in this sample, as well as a small amount of mesopores of ca. 20 nm, possibly ascribable to a certain amount of C-S-H phases formed by a lime-aggregate. Essays carried out after 28 and 91 days of curing for this same sample showed that the porous structure was retained with a similar distribution to that of the critical diameter and the area of the largest macropores. However, the mesoporosity of 20 nm disappeared after 28 days (Fig. 2b and 2c). Carbonation of C-S-H compounds could have occluded this range of pores.

The pore distribution and the critical diameter attained after water removing by freeze-drying of MS1 samples were similar to those observed by the solvent exchange procedure. A macroporous region was also noted, between 5 and 20 μm (Fig. 2d), which was maintained at 28 days (Fig. 2e)

but decreased after 91 days of curing (Fig. 2f). This last fact was a probable consequence of the carbonation advance which could block a part of these pores. The dry weight percentage of calcium carbonate referred to the initial sample, as determined by thermogravimetric analysis, varied in the samples treated from 5.7% (7 days), to 11.2% (28 days) and to 14.4% (91 days), thus corroborating the carbonation progress as the main reason that explains the modification of the pore structure. Although a more accurate assessment of the mesopores will be tackled below, by MIP the mesopores at ca. 20 nm maintains a similar pattern to that of the samples treated with isopropanol. It is worth mentioning that the initial mercury requirement to fill the larger spaces between particles turned out to be larger in the freeze-dried sample than in the sample treated by the solvent exchange method. This circumstance could point to the freeze-drying method as a more effective way to remove the water.

When vacuum drying was used, a reduction in the macroporous area was observed for 7-day cured samples (Fig. 2g) compared to the two previously discussed drying methods, whereas the critical diameter for the porous structure remained ca. 0.6 μm. The initial mercury demand to fill the interparticle space was dramatically reduced. Moreover, after 28 days of curing, macropores appeared in the range of 5 to 20 μm (Fig. 2h). This macroporosity had not been detected in the 7-days old sample. These facts suggest the inability of the vacuum drying method to completely remove any excess water: at day 28, the passing of time and the subsequent water evaporation allowed the development of undetected, formerly water-filled pores.

Oven drying at 60 ° C did not differ much from the previous procedures, at least after 7 and 28 days of curing, and maintained the critical diameter at *ca.* 0.6 μm (Fig. 2j and 2k). However, the curve of pore size distribution drastically changed after 91 days of curing (Fig. 2l), so that the critical diameter shifted to nearly 1 μm and previously unnoticed macropores appeared between 10 and 40

μm. It seems that the drying conditions favored a forced dehydration of the material with microstructural consequences. The same observation is clearer after drying at 105 °C (Fig. 2m and 2n): after 28 days, the critical diameter reached almost 1 μm, and no pores under 30 nm were measurable. The high heating temperature may lead to irreversible collapse of the gel pores due to interlayer water loss, as described for cement binding systems. The increase in macroporosity after applying oven drying methods has also been reported in previous works dealing with drying methods in cement pastes and mortars as a consequence of stresses caused by surface tension-related phenomena. It seems that, during the pore emptying, the receding water menisci lead to a collapse of some of the fine pores, thus increasing the number of larger pores [36].

Specific surface area measurements were used by applying the BET method to the N_2 adsorption isotherms data to check and confirm the results described above on the effects of the drying methods in the microstructure of the samples (Table 1). These results were also useful in order to compare and prove the efficiency of the different water removal procedures by comparison with untreated samples. The largest specific areas were generally found –for any assayed curing period- for the samples subjected to freeze-drying, followed by those which underwent the exchange process with isopropanol. Drying at 105 °C generated a slightly lower surface area, but was associated with the problems of structural changes discussed above. Both vacuum and oven drying at 60 °C proved significantly less efficient methods, usually yielding smaller surface areas. It must be considered that too low surface area values would be measured if the drying process partially destroys or alters the C–S–H gel structure [37]. It can thus be inferred that freeze-drying and solvent-exchange methods yielded the best results according to specific surface area data.The MS1 samples that did not undergo any drying procedure (non-dried samples), however, systematically yielded the lowest specific surface area values at each period of curing. This fact evidences the need for a water removal method previous to any assessment of the microstructure of lime binding matrix.

TG analysis carried out on MS1 samples subjected to the five different drying procedures showed that the degree of carbonation increased with curing days, in good agreement with MIP observations, which resulted in occlusion of pores and in a decrease in the specific surface. Taking into account the values obtained after the five treatments of drying, the average contents of $CaCO_3$ were 5.5% after 7 curing days, 13.2% after 28 curing days and 16.2% after 91 days. At the same time, the amount of uncarbonated calcium hydroxide underwent a gradual reduction: 14.9% at 7 days, 9.5% at 28 days and, finally, 3.4% after 91 curing days. Complete carbonation of aerial lime mortars cannot be achieved even after long curing periods [20].

Although in some studies on cements it has been stated that freeze-drying affects the crystallinity of some hydrates and therefore their pore structure, making solvent exchange the best choice [34,46], this problem seems substantially less significant in lime-based mixtures. Given the greater overall porosity in aerial lime mortars and the absence of hydrates - except those that may appear in the form of C-S-H phases, which are only relevant on pozzolanic additions – water expansion in the instantaneous freezing process prior to sublimation is easier to accommodate.

In the presence of NS, the PSD pattern and the effect of the drying process on the PSD structure measured by MIP were seen to partially resemble the effect observed in plain aerial lime samples (Fig. 3).

The critical pore diameter remained ca. 0.6 μm (Fig. 3a, 3b, 3c and 3d) although, as in the case of MS1 samples (Fig. 2n), oven drying at 105 °C shifted it towards a value closer to 1 μm (Fig. 3e). Macropores with diameters between 2 and 10 μm approx. were detected. However, after 28 days of curing, drying in an oven -especially at 105 °C, as also happened in the MS1 samples- increased the

329 macroporosity between 10 and 40 μm, ascribable to an abrupt dehydration that resulted in the
330 appearance of cracks in the matrix (Fig. 3e). After 91 days, the curves became smooth and
331 macroporosity was not so evident, since removal of excess water proceeded more gradually along
332 with carbonation. In general, all MS2 samples showed a slightly lower porosity than MS1 samples,
333 giving rise to a more compact material. However, despite the reduction in total porosity, an increase
334 in specific surface area was observed for MS2 samples as a result of the incorporation of a 3 wt. %
335 NS, a nanostructured material with large surface area [21]. As an example, Table 2 collects a
336 comparative study of the specific surface area for the three batches of samples after 7 curing days. It
337 can be seen that MS2 samples, in general, yielded larger specific surface areas than MS1 samples.
338
339 Furthermore, specific surface area measurements of MS2 samples carried out under the different
340 drying procedures followed the trend of the MS1 samples, where the exchange with isopropanol and
341 the freeze-drying provided the highest drying efficiencies, as expressed in terms of a larger surface
342 area available for adsorption of nitrogen at 77 K.
343
344 It was expected that NS could react with the $Ca(OH)_2$ particles giving rise to the formation of C-S-H
345 phases [24,28]. Curiously, after performing many of the drying procedures, the foreseeable porosity
346 due to the C-S-H phases, meso- and micropores (pores < 50 nm, [29]) could not be detected by MIP
347 (see Fig. 3). From TG results for MS2 samples the obtained average $Ca(OH)_2$ percentages were
348 13.0%, after 7 curing days, 5.5% after 28 days of curing and 2.9% after 91 days. As evidenced by
349 the results, the $Ca(OH)_2$ contents in MS2 samples dropped at higher rate than those observed for
350 MS1 samples. This fact indicates that $Ca(OH)_2$ consumption was due not only to the carbonation
351 process but to the pozzolanic-type reaction between NS and $Ca(OH)_2$ particles as well [47].
352 Therefore, C-S-H formation cannot be ruled out and will be confirmed below in a detailed study of
353 the meso- and microporous area. Besides the lower accuracy of MIP technique for the assessment of

the mesopores range, the absence of significant mesoporosity in MIP results can be related to the small particle size of the added nanosilica. NS may behave as nanofiller, thus drastically reducing the measured volume by MIP in the mesopores range. This fact will be discussed in depth below.

By incorporating the required amount of mixing water to achieve adequate workability after the addition of NS, experiments in the series of MS3 samples confirmed previous observations in MS2 series regarding the pore size distribution obtained by MIP. Thus, the critical diameter remained centered around 0.6 μm, the specimens showed moderate porosity in the 6 to 10 μm range as well as a not very marked porosity in the most mesoporous region. The comparative analysis of the results obtained by following the different drying procedures shows that both isopropanol exchange and freeze-drying yielded similar curves at 7 days. After 28 curing days (Fig. 4a and 4b), some of these MS3 samples showed a marked increase in macroporosity and, at the same time, a shift in the critical diameter to sizes close to 1 μm. Most probably, the larger amount of mixing water available generated, after its removal, a parallel increase in the number of large pores (see, as an example, Fig. 4a).

The vacuum drying procedure after 7 days of curing generated a pore size distribution curve similar to the previous two procedures. The filling effect of NS above described yielded small porosity that was almost undetectable by MIP. At 28 days, this drying process also caused a significant increase in 20 - 40 μm macropores (Fig. 4b). A similar behavior was observed when drying was conducted in an oven at either 60° or 105 ° C: noticeable changes in the pore size distribution occur after 28 days of curing, with an outstanding macroporosity that could be associated with dehydration of the material with structural changes that are, usually, accompanied by an increase in the critical diameter, which marks the access of mercury to the interconnected network of pores.

The specific surface area data matched well these observations, the largest available specific surface areas being provided by either exchange with isopropanol or freeze- drying, and, to a lesser extent, the other three assayed methods (see Table 2). The MS3 series showed, in general, the highest specific surface area values, in line with those obtained for MS2 samples, thus confirming that the incorporation of NS renders high specific surface area in lime binding materials.

3.2. Assessment of the micro and mesoporous structure

An accurate evaluation of the pore size distribution of the mesopores area, specifically from 1.7 to 300 nm, was carried out with the data obtained by nitrogen adsorption isotherms at 77 K, and subsequent interpretation of results by means of the BJH method [14].

For the MS1 series, after 7 days of curing, pores in the aforementioned range can be appreciated, with one major peak between 45 and 60 nm (Fig. 5a).

The largest critical diameter (around 60 nm) was achieved by drying in an oven at 105 °C, which yielded a poorly refined and very irregular PSD. Within 28 days of curing the differences are even greater. In general, porosity below 10 nm underwent a reduction, and it was only noticeable when either solvent exchange or freeze-drying was used (shown in Fig. 5b as a small peak at ca. 4 nm). A combined action of carbonation and drying shrinkage, which reduced the interparticle space, could be held responsible for the disappearance of this small pores after applying the vacuum and oven (60 and 105ºC) drying processes. However, solvent exchange and freeze-drying procedures are able to efficiently remove the water trapped in these small gel pores related to the formation of a certain amount of C-S-H phases. The porosity below 50 nm was very poorly observed with the vacuum and oven drying at 105°C, much information being lost (Fig. 5b).

After subjecting the samples to 91 days of curing (Fig. 5c), the porous structure analysis using the curves obtained by the BJH method revealed that the porosity below 50 nm was reduced by half in the samples studied, a phenomenon which, as has been mentioned in the preceding paragraph, can be attributed to the closing of pores by both ongoing carbonation and shrinkage. This finding can be clearly seen in Fig. 6, which shows as an example the PSD of freeze-dried samples after 7, 28 and 91 curing days. Long-term curing allowed all remaining free water to evaporate, so that differences between the various drying methods were lessened, as observed in the PSD (Fig. 5c).

When comparing MS2 samples (3 wt. % added NS), with MS1 samples (NS-free), a larger population of pores <10 nm, gel capillaries, was found for the former, as Fig. 7 shows for MS2 samples after 7 curing days. Specifically, the average volume of pores less than 10 nm expressed in mm^3 per gram of sample increased from 1.71 in MS1 series to 3.25 in MS2 series. Therefore, the formation of C-S-H compounds in MS2 samples was evidenced by the detection of these gel pores [29,40,41]. This increase in the amount of pores <10 nm is in line with that observed for cement-NS composites [21] and also for aerial lime-metakaolin mortars [9]. Furthermore, a comparative SEM analysis was carried out for MS1 (Fig. 8a and 8b) and MS2 samples (Fig. 8c to 8g). The MS1 samples showed large porosity and agglomerations of scaleno-rhombohedral calcite crystals (Fig. 8a) together with some hexagonal plate-like crystals of uncarbonated portlandite ($Ca(OH)_2$) (Fig. 8b) [48]. The NS addition clearly resulted in a pore size reduction in MS2 samples (Fig. 8c). NS-lime reaction in MS2 samples resulted in a $Ca(OH)_2$ consumption, preventing the portlandite crystals from identification, together with the appearance of some thin foil and honeycomb-shaped C-S-H structures (Fig. 8d). C-S-H fibers can be observed in Fig. 8e. In Fig. 8f, the textural characteristics of the sample shows that the binding matrix clearly presents a nanosized porosity, with a compact binding matrix. Finally, Fig. 8g depicts, in the center of the micrograph, an agglomeration of C-S-H

compounds that allows us to observe pores sized in the nanometer range. The chemical composition of these compounds was established by means of EDS analysis, which yielded Ca, Si and O in their composition (see, as an example, the EDS analysis graph of the agglomeration depicted in Fig. 8g).

Among the different assayed drying methods with MS2 samples, again freeze-drying and solvent exchange proved to be most sensitive in the determination of pores below 25 nm, as shown in Fig. 7, in which this pore range is broader and easier to detect when using the two mentioned drying methods. Contrary to the peak-shaped PSD observed in the MS1 samples (with maximum between 45-60 nm), the PSD of MS2 samples presented a plateau above ca. 15 to 150 nm. As an example, the PSD graphs of samples of the three series (MS1, MS2 and MS3) after 7 curing days subjected to solvent-exchange and freeze-drying methods are depicted in Fig. 9a and 9b, respectively. It must be emphasized that such a notable change in the PSD of micro- and mesopores was caused by the addition of just 3 wt. % NS with respect to the plain lime specimen. These changes can be well understood assuming the aforementioned role as nanofiller of the nanosilica incorporated into the MS2 samples. The presence of NS reduced the number of large and medium capillary pores in the approximate range of 20 to 100 nm (the average pore volume of that range expressed in mm^3 per gram of sample decreased from 18.64 to 11.17), as a result of the fact that silica nanoparticles were interspersed between the lime particles. These results are in good agreement with the MIP data, in which – as above discussed – in spite of the fact of NS addition, a negligible amount of pores lower than 100 nm was detected. The presence of intercalated NS particles resulted in a wider PSD but with smaller pores, with maximum population from 10 to 15 nm (Fig. 9).

This filling role of the NS could be also confirmed in the MS3 series of samples (lime mortars with added NS but with a large amount of mixing water). As an example, Fig. 10 shows the distributions of the pore sizes of MS3 samples after 7 curing days, including the PSD of a non-dried sample,

454 which reveals that, without applying a drying procedure, a large amount of mesopores are blocked
455 and cannot be evaluated. The PSD of MS3 samples also followed the same trend as in MS2 samples:
456 the presence of NS caused a reduction in the pores ranging from 20 to 100 nm, while it increased the
457 pores below 15 nm, in comparison with MS1 samples depicted in Fig. 5. As in the case of MS2
458 samples, freeze-drying and solvent exchange were the drying methods that most effectively allowed
459 us to assess this last range of pores. Also Fig. 9 shows that MS3 behaved in a similar way to MS2,
460 proving that NS acted as nanofiller in both series of samples.
461
462 Concurrently, the presence of NS and its reaction with lime, forming calcium silicates which are
463 subsequently hydrated, was helpful to increase the population of the gel pores (pores sized below 10
464 nm), by formation of C-S-H phases in MS2 as well as in MS3 batches of samples. These pores
465 partially collapsed and disappeared when the NS-containing samples were cured for 28 days and
466 later, as a result of the ongoing carbonation and/or the shrinkage process.
467
468 All these facts were confirmed by a micropore analysis by using the Hovarth-Kawazoe approach.
469 The maximum pore volume values (in the range from 0.5 to 1.7 nm) obtained by this method in
470 specimens after 7 curing days revealed that, upon the addition of NS, micropore volume data
471 underwent an increase of ca. 30% in samples subjected to solvent-exchange or freeze-drying
472 method, proving the formation of C-S-H gel pores (Table 3). Among the different drying methods,
473 both solvent-exchange and freeze-drying effectively removed the water allowing us to measure this
474 pore range appropriately. After 28 curing days, the ongoing carbonation caused a decrease in the
475 maximum pore volume of the micropore population of 57% on average. HK analysis indicated that
476 the mean pore width in the micropore region was around 1 nm.
477

The consequences of (i) the filling role of the NS, as evidenced by PSD measurements, and (ii) the C-S-H development owing to the pozzolanic reaction, achieve their greatest exponent in the outstanding increase of the compressive strength values after the NS addition. Table 4 shows the compressive strength values for non-dried samples comparing MS1 samples with MS2 and MS3. After 28 curing days, the compressive strength of MS2 specimens increased by ca. 172% in comparison with MS1 samples. As for MS3 samples, 28-day compressive strength underwent a rise of 139% with respect to MS1 samples. Longer curing times (91 days) resulted in a compressive strength increase ranging from 122% to 136%.

Upon the addition of larger amounts of NS (6 wt.%), the compressive strength increase was greater, proving the advantageous effect of adding NS to lime binding matrix. After 91 curing days, compressive strength results tripled or quadrupled the values of the control group of samples, depending on the amount of mixing water explained by the differences between MS2- and MS3-type samples [28].

4. Conclusions

The addition of nanosilica to a lime-based binding material changed dramatically the mesopore distribution due to the proven behavior as nanofiller that caused a decrease of the pores in the range 20-100 nm. Nanosilica was interspersed between the lime particles. This is the first study in which the NS behavior as nanofiller in a lime-based matrix has been shown by a thorough analysis of the pore structure. Besides, the NS incorporation induced C-S-H development, giving rise to an enriched population of gel pores (< 10 nm), including the micropore range. These two facts resulted in clearly improved mechanical strength in the samples and may have relevant practical purposes in order to enhance the compressive strength of aerial lime mortars.

Among the five assayed drying methods, freeze-drying and solvent exchange methods have been proven to render the specimens in optimum conditions for subsequent porous structure and specific surface area analysis by means of both MIP and N_2 adsorption isotherms. Samples subjected to these two methods had the greatest water removal, as shown by the fact that they had the highest values of specific surface area, while keeping their pore size distribution unaltered.

Oven drying at 105ºC altered the macropore area of the lime mixtures and was not able to bring about complete water removal. Subsequent analysis of the micro and mesoporous area, was hindered specially that of the C-S-H gel pores (pore size < 10 nm) formed after pozzolanic additions. The specific surface area values achieved by this method were lower than those obtained by either solvent exchange or freeze-drying methods. Oven drying at 60ºC and vacuum drying methods were found inefficient to effectively remove the excess water, so that the micropore, mesopore and macropore range could not be properly analyzed. Considering all the studied methods, only freeze-drying allowed us to gather data in a reasonable period of time, while the others were time-consuming.

Acknowledgements

The authors want to thank CTH Navarra, Calinsa S.A. Navarra and Ulmen Europa S.L. for the material supplied. They also gratefully acknowledge Dr. M.C. Jiménez de Haro (ICMS) for her assistance in the SEM analysis. This work was funded by FUNA (Fundación Universitaria de Navarra) under project number FUNA2012-15108172.

References

[1]. A. Arizzi, H. Viles, G. Cultrone, Experimental testing of the durability of lime-based mortars used for rendering historic buildings, Constr. Build. Mater. 28 (2012) 807-818.

[2]. G. Margalha, R. Veiga, A. Santos Silva, J. de Brito, Traditional methods of mortar preparation: The hot lime mix method, Cem. Concr. Compos. 33 (2011) 796-804.

[3]. H. Paiva, A. Velosa, R. Veiga, V.M. Ferreira, Effect of maturation time on the fresh and hardened properties of an air lime mortar, Cem. Concr. Res. 40 (2010) 447-451.

[4]. A. Izaguirre, J. Lanas, J.I. Álvarez, Behaviour of a starch as a viscosity modifier for aerial lime-based mortars, Carbohydr. Polym. 80 (2010) 222-228.

[5]. I. Karatasios, M.S. Katsiotis, V. Likodimos, A.I. Kontos, G. Papavassiliou, P. Falaras, V. Kilikoglou, Photo-induced carbonation of lime-TiO2 mortars, Applied Catalysis B: Environmental 95 (2010) 78-86.

[6]. A. Izaguirre, J. Lanas, J.I. Álvarez, Effect of water-repellent admixtures on the behaviour of aerial lime-based mortars Cem. Concr. Res. 39 (2009) 1095-1104.

[7]. A. Izaguirre, J. Lanas, J.I. Álvarez, Characterization of aerial lime-based mortars modified by the addition of two different water-retaining agents, Cem. Concr. Compos. 33 (2011) 309-318.

[8]. A. El-Turki, R.J. Ball, S. Holmes, W.J. Allen, G.C. Allen, Environmental cycling and laboratory testing to evaluate the significance of moisture control for lime mortars, Constr. Build. Mater. 24 (2010) 1392-1397.

[9]. A. Arizzi, G. Cultrone, Aerial lime-based mortars blended with a pozzolanic additive and different admixtures: A mineralogical, textural and physical-mechanical study,Constr. Build. Mater. 31 (2012) 135-143.

[10]. G. Wei, H. Zhang, H. Wang, S. Fang, B. Zhang, F. Yang, An experimental study on application of sticky rice–lime mortar in conservation of the stone tower in the Xiangji Temple, Constr. Build. Mater. 28 (2012) 624-632.

552 [11]. L. Ventolà, M. Vendrell, P. Giraldez, L. Merino, Traditional organic additives improve lime
553 mortars: New old materials for restoration and building natural stone fabrics, Constr. Build.
554 Mater. 25 (2011) 3313-3318.
555 [12]. M.P. Seabra, H. Paiva, J.A. Labrincha, V.M. Ferreira, Admixtures effect on fresh state
556 properties of aerial lime based mortars, Constr. Build. Mater. 23 (2009) 1147-1153.
557 [13]. E. Aggelakopoulou, A. Bakolas, A. Moropoulou, Properties of lime–metakaolin mortars for
558 the restoration of historic masonries, Appl. Clay Sci. 53 (2011) 15-19.
559 [14]. M. Tziotziou, E. Karakosta, I. Karatasios, G. Diamantopoulos, A. Sapalidis, M. Fardis, P.
560 Maravelaki-Kalaitzaki, G. Papavassiliou, V. Kilikoglou, Application of ^{1}H NMR to hydration
561 and porosity studies of lime–pozzolan mixtures, Micropor. Mesopor. Mat. 139 (2011) 16-24
562 [15]. A. Gameiro, A. Santos Silva, R. Veiga, A. Velosa, Hydration products of lime–metakaolin
563 pastes at ambient temperature with ageing, Thermochim. Acta 535 (2012) 36-41.
564 [16]. E. Vejmelková, M. Keppert, P. Rovnaníková, Z. Keršner, R. Černý, Application of burnt clay
565 shale as pozzolan addition to lime mortar, Cem. Concr. Compos. 34 (2012) 486-492.
566 [17]. A. Sepulcre-Aguilar, F. Hernández-Olivares, Assessment of phase formation in lime-based
567 mortars with added metakaolin, Portland cement and sepiolite, for grouting of historic masonry,
568 Cem. Concr. Res. 40 (2010) 66-76.
569 [18]. C. Fortes-Revilla, S. Martínez-Ramírez, M.T. Blanco-Varela, Modelling of slaked lime–
570 metakaolin mortar engineering characteristics in terms of process variables, Cem. Concr.
571 Compos. 28 (2006) 458-467.
572 [19]. N. Billong, U.C. Melo, D. Njopwouo, F. Louvet, J.P. Bonnet, Effect of mixture constituents
573 on properties of slaked lime–metakaolin–sand mortars containing sodium hydroxide, Cem.
574 Concr. Compos. 31 (2009) 658-662.
575 [20]. J Lanas, J.I. Alvarez-Galindo, Masonry repair lime-based mortars: factors affecting the
576 mechanical behavior, Cem. Concr. Res. 33 (2003) 1867-1876.

577 [21]. J-Y. Shih, T-P. Chang, T-C. Hsiao, Effect of nanosilica on characterization of Portland
578 cement composite, Mat. Sci. Eng. A-Struct. 424 (2006) 266–274.
579 [22]. G. Quercia, G. Hüsken, H.J.H. Brouwers, Water demand of amorphous nano silica and its
580 impact on the workability of cement paste, Cem. Concr. Res. 42 (2012) 344-357.
581 [23]. M-H. Zhang, J. Islam, Use of nano-silica to reduce setting time and increase early strength of
582 concretes with high volumes of fly ash or slag, Constr. Build. Mater. 29 (2012) 573-580.
583 [24]. F. Kontoleontos, P.E. Tsakiridis, A. Marinos, V. Kaloidas, M. Katsioti, Influence of colloidal
584 nanosilica on ultrafine cement hydration: Physicochemical and microstructural characterization,
585 Constr. Build. Mater. 35 (2012) 347-360.
586 [25]. P. Hou, S. Kawashima, K. Wang, D.J. Corr, J. Qian, S.P. Shah, Effects of colloidal
587 nanosilica on rheological and mechanical properties of fly ash-cement mortar, Cem. Concr.
588 Compos. 2012, doi: http://dx.doi.org/10.1016/j.cemconcomp.2012.08.027.
589 [26]. J. Björnström, A. Martinelli, A. Matic, L. Börjesson, I. Panas, Accelerating effects of
590 colloidal nano-silica for beneficial calcium–silicate–hydrate formation in cement, Chem. Phys.
591 Lett. 392 (2004) 242–248.
592 [27]. M. Berra, F. Carassiti, T. Mangialardi, A.E. Paolini, M. Sebastiani, Effects of nanosilica
593 addition on workability and compressive strength of Portland cement pastes, Constr. Build.
594 Mater. 35 (2012) 666–675.
595 [28]. J.M. Fernández, A. Durán, I. Navarro-Blasco, J. Lanas, R. Sirera, J.I. Alvarez, Influence of
596 nanosilica and a polycarboxylate ether superplasticizer on the performance of lime mortars,
597 Cem. Concr. Res. 43 (2013) 12-24.
598 [29]. R.M. Espinosa, L. Frank, Influence of the age and drying process on pore structure and
599 sorption isotherms of hardened cement paste, Cem. Concr. Res. 36 (2006) 1969–1984.
600 [30]. M. Stefanidou, Methods for porosity measurement in lime-based mortars,
601 Constr. Build. Mater. 24 (2010) 2572-2578.

602 [31]. M. Arandigoyen, J.I. Alvarez, Blended pastes of cement and lime: Pore structure and
603 capillary porosity, Appl. Surf. Sci. 252 (2006) 8077-8085.
604 [32]. M. Arandigoyen, B. Bicer-Simsir, J.I. Alvarez, D.A. Lange, Variation of microstructure with
605 carbonation in lime and blended pastes, Appl. Surf. Sci. 252 (2006) 7562-7571.
606 [33]. J. Zhang, G.W. Scherer, Comparison of methods for arresting hydration of cement, Cem.
607 Concr. Res. 41 (2011) 1024-1036.
608 [34]. N.C. Collier, J.H. Sharp, N.B. Milestone, J. Hill, I.H. Godfrey, The influence of water
609 removal techniques on the composition and microstructure of hardened cement pastes, Cem.
610 Concr. Res. 38 (2008) 737-744.
611 [35]. L. Konecny, S.J. Naqvi, The effect of different drying techniques on the pore size
612 distribution of blended cement mortars, Cem. Concr. Res. 23 (1993) 1223–1228.
613 [36]. C. Gallé, Effect of drying on cement-based materials pore structure as identified by mercury
614 intrusion porosimetry: A comparative study between oven-, vacuum-, and freeze-drying, Cem.
615 Concr. Res. 31 (2001) 1467-1477.
616 [37]. A. Korpa, R. Trettin, The influence of different drying methods on cement paste
617 microstructures as reflected by gas adsorption: Comparison between freeze-drying (F-drying),
618 D-drying, P-drying and oven-drying methods, Cem. Concr. Res. 36 (2006) 634-649.
619 [38]. M. Arandigoyen, J.L. Pérez Bernal, M.A. Bello López, J.I. Alvarez, Lime-pastes with
620 different kneading water: Pore structure and capillary porosity, Appl. Surf. Sci. 252 (2005) 1449-
621 1459.
622 [39]. R.M. Lawrence, T.J. Mays, S.P. Rigby, P. Walker, D. D'Ayala, Effects of carbonation on the
623 pore structure of non-hydraulic lime mortars, Cem. Concr. Res. 37 (2007) 1059-1069.
624 [40]. P. Pipilikaki, M. Beazi-Katsioti, The assessment of porosity and pore size distribution of
625 limestone Portland cement pastes, Constr. Build. Mater. 23 (2009) 1966–1970.

626 [41]. N. De Belie, J. Kratky, S. Van Vlierberghe, Influence of pozzolans and slag on the
627 microstructure of partially carbonated cement paste by means of water vapour and nitrogen
628 sorption experiments and BET calculations, Cem. Concr. Res. 40 (2010) 1723-1733.
629 [42]. J. Dweck, P.M. Buchler, A.C. Vieira-Coelho, F.K. Cartledge, Hydration of a Portland cement
630 blended with calcium carbonate, Thermochim. Acta 346 (2000) 105–113.
631 [43]. A. Duran, L.A. Perez-Maqueda, J. Poyato, J.L. Perez-Rodriguez, A termal study approach to
632 romana ge wall painting mortars, J. Therm. Anal. Calorim. 99 (2010) 803-809.
633 [44]. C.A. García-González, N. el Grouh, A. Hidalgo, J. Fraile, A.M. López-Periago, C. Andrade,
634 C. Domingo, New insights on the use of supercritical carbon dioxide for the accelerated
635 carbonation of cement pastes, J. Supercrit. Fluid. 43 (2008) 500-509.
636 [45]. S. Goñi, M. Frias, I. Vegas, R. García, R. Vigil de la Villa, Quantitative correlations among
637 textural characteristics of C–S–H gel and mechanical properties: Case of ternary Portland
638 cements containing activated paper sludge and fly ash, Cem. Concr. Compos. 34 (2012) 911-
639 916.
640 [46]. C. Gosselin, E. Gallucci, K. Scrivener, Influence of self heating and Li_2SO_4 addition on the
641 microstructural development of calcium aluminate cement, Cem. Concr. Res. 40 (2010) 1555-
642 1570.
643 [47]. S. Kawashima, P. Hou, D.J. Corr, S.P. Shah, Modification of cement-based materials with
644 nanoparticles, Cem. Concr. Compos. (2012) http://dx.doi.org/10.1016/j.cemconcomp.
645 2012.06.01.
646 [48]. O. Cizer, C. Rodriguez-Navarro, E. Ruiz-Agudo, J. Elsen, D. Van Gemert, K. Van Balen,
647 Phase and morphology evolution of calcium carbonate precipitated by carbonation of hydrated
648 lime, J. Mater. Sci. 47 (2012) 6151–6165.
649

Table 1. BET specific surface area (m^2g^{-1}) for MS1 samples subjected to different water removal procedures after various curing periods. Values obtained for a non-dried sample are also shown for comparison purposes.

Procedure	*7 curing days*	*28 curing days*	*91 curing days*
Non - dried	2.65 ± 0.02	2.15 ± 0.01	1.28 ± 0.01
Solvent - exchange	4.07 ± 0.02	3.45 ± 0.01	1.83 ± 0.01
Freeze - drying	4.56 ± 0.04	3.43 ± 0.03	1.97 ± 0.01
Vacuum drying	3.31 ± 0.03	2.25 ± 0.01	1.53 ± 0.02
Oven drying 60ºC	3.42 ± 0.02	2.99 ± 0.03	1.76 ± 0.02
Oven drying 105ºC	3.93 ± 0.01	3.11 ± 0.01	1.80 ± 0.01

Table 2. BET specific surface area (m^2g^{-1}) for samples subjected to the five different water removal procedures after 7 curing days.

Procedure	*MS1*	*MS2*	*MS3*
Solvent - exchange	4.07 ± 0.02	5.41 ± 0.01	5.87 ± 0.01
Freeze - drying	4.56 ± 0.04	5.30 ± 0.01	5.39 ± 0.01
Vacuum drying	3.31 ± 0.03	3.53 ± 0.03	3.67 ± 0.03
Oven drying 60ºC	3.42 ± 0.02	3.60 ± 0.01	3.58 ± 0.02
Oven drying 105ºC	3.93 ± 0.01	3.27 ± 0.01	3.50 ± 0.01

Table 3. Maximum micropore volume (mm^3g^{-1}) -calculated through the Hovarth-Kawazoe approach- in specimens subjected to the five different drying procedures after 7 days of curing.

Procedure	***MS1***	***MS2***	***MS3***
Solvent - exchange	1.48 ± 0.02	1.90 ± 0.01	2.09 ± 0.01
Freeze - drying	1.45 ± 0.02	1.94 ± 0.01	1.91 ± 0.01
Vacuum drying	1.31 ± 0.02	1.19 ± 0.02	1.41 ± 0.02
Oven drying 60ºC	1.24 ± 0.01	1.32 ± 0.02	1.34 ± 0.02
Oven drying 105ºC	1.35 ± 0.02	1.15 ± 0.02	1.15 ± 0.02

Table 4. Compressive strength results (MPa).

Curing days	*MS1*	*MS2*	*MS3*	*MS2 6%NS*[a]	*MS3 6%NS*[a]
7	0.36 ± 0.02	0.86 ± 0.02	0.71 ±0.01	1.54 ± 0.06	0.94 ± 0.02
28	0.67 ± 0.13	1.83 ± 0.13	1.61 ± 0.04	3.22 ± 0.18	1.96 ± 0.06
91	1.07 ± 0.28	2.38 ± 0.28	2.52 ± 0.27	4.28 ± 0.05	2.89 ± 0.01

[a]Samples with the same compositions as those of MS2 and MS3 series but loaded with 6% wt. NS

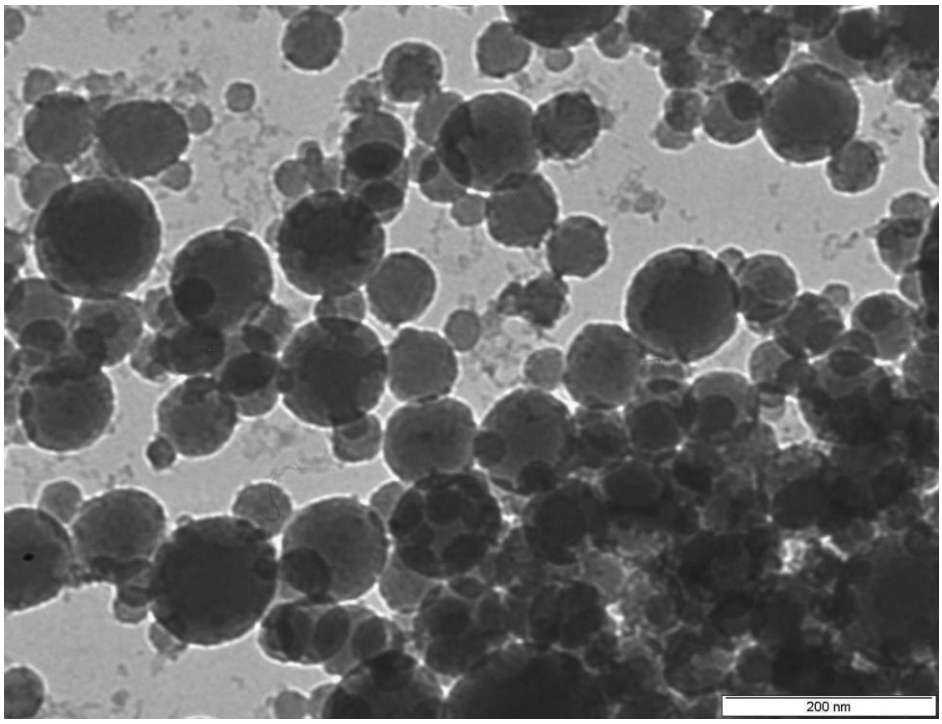

Figure 1. TEM micrograph of NS particles.

High-resolution Figure2

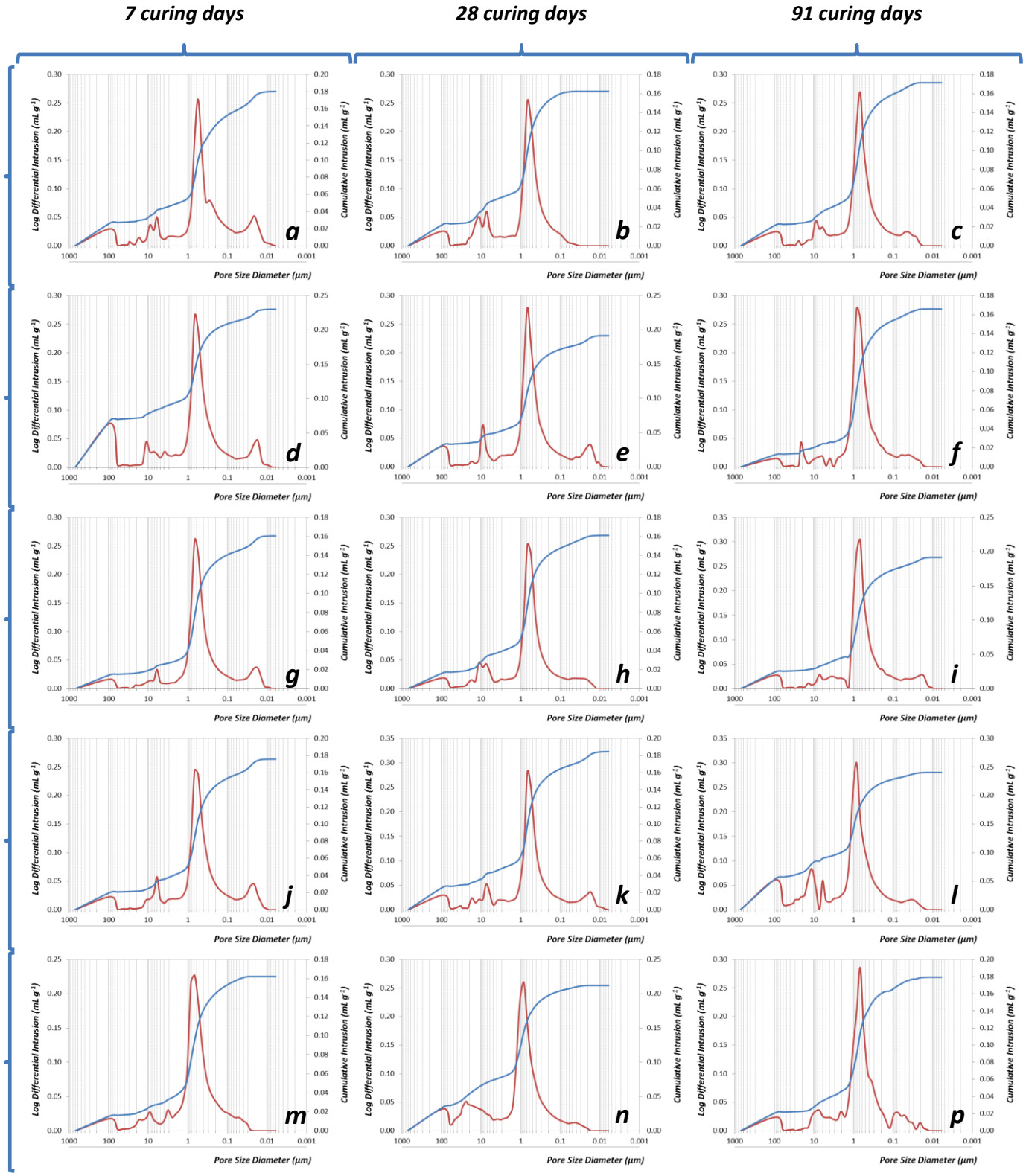

Figure 2. Differential pore size distribution and Hg-intrusion cumulative curves obtained by MIP of MS1 samples subjected to different water removal procedures:

solvent-exchange drying method (a, b, c), freeze-drying (d,e,f), vacuum drying (g, h, i), oven drying at 60ºC (j, k, l) and oven drying at 105ºC (m, n, o), after 7, 28 and 91 curing days, respectively.

Figure 3 rv

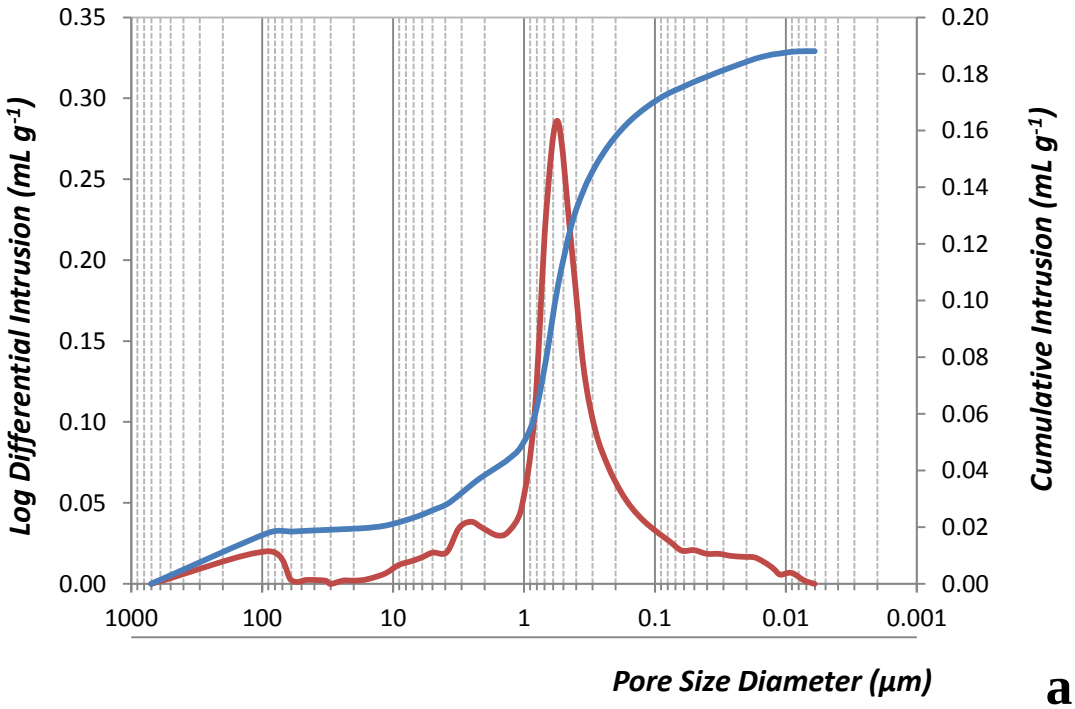

a

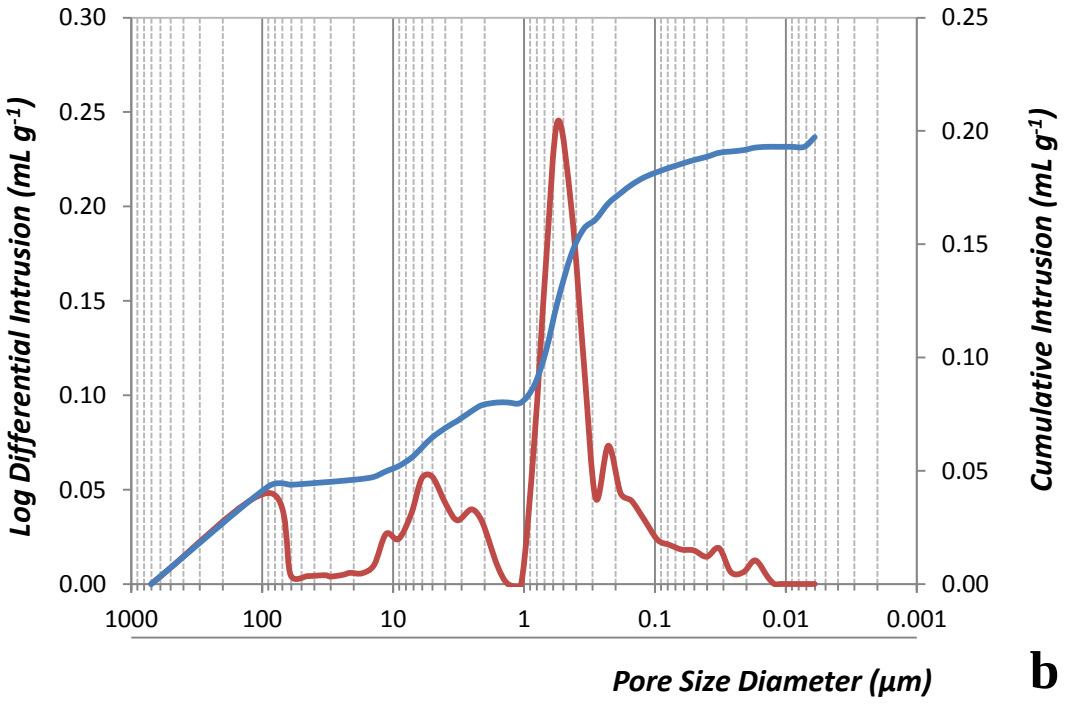

b

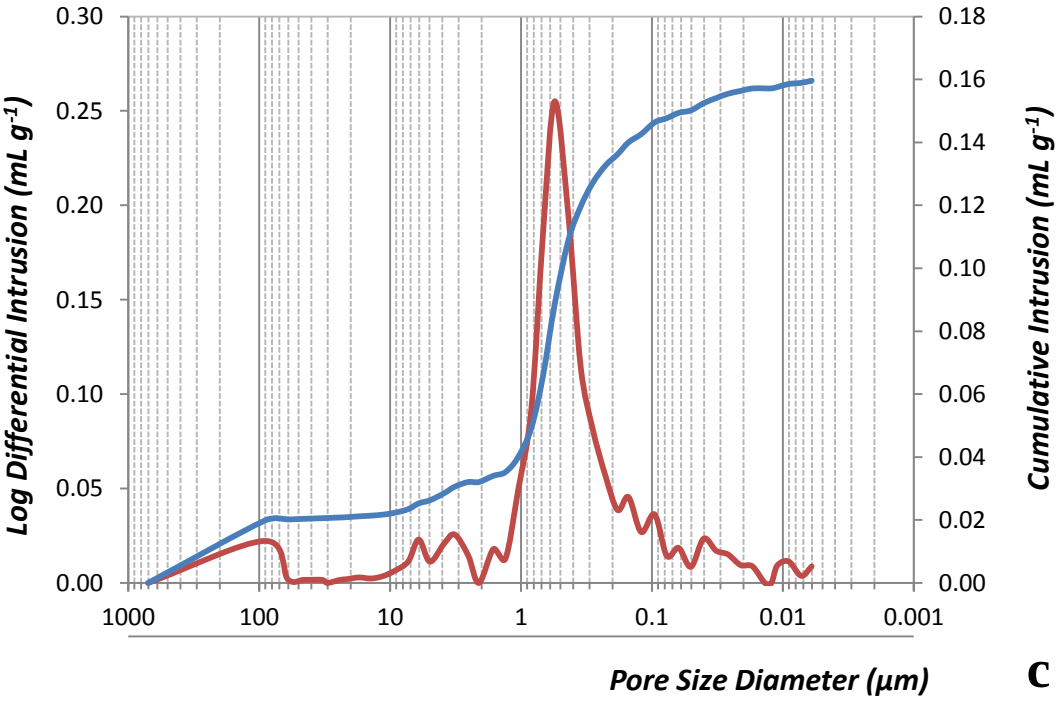
0.30
0.25
0.20
0.15
0.10
0.05
0.00
0.18
0.16
0.14
0.12
0.10
0.08
0.06
0.04
0.02
0.00
1000
100
10
1
0.1
0.01
0.001
Log Differential Intrusion (mL g-1)
Cumulative Intrusion (mL g-1)
Pore Size Diameter (µm)

c

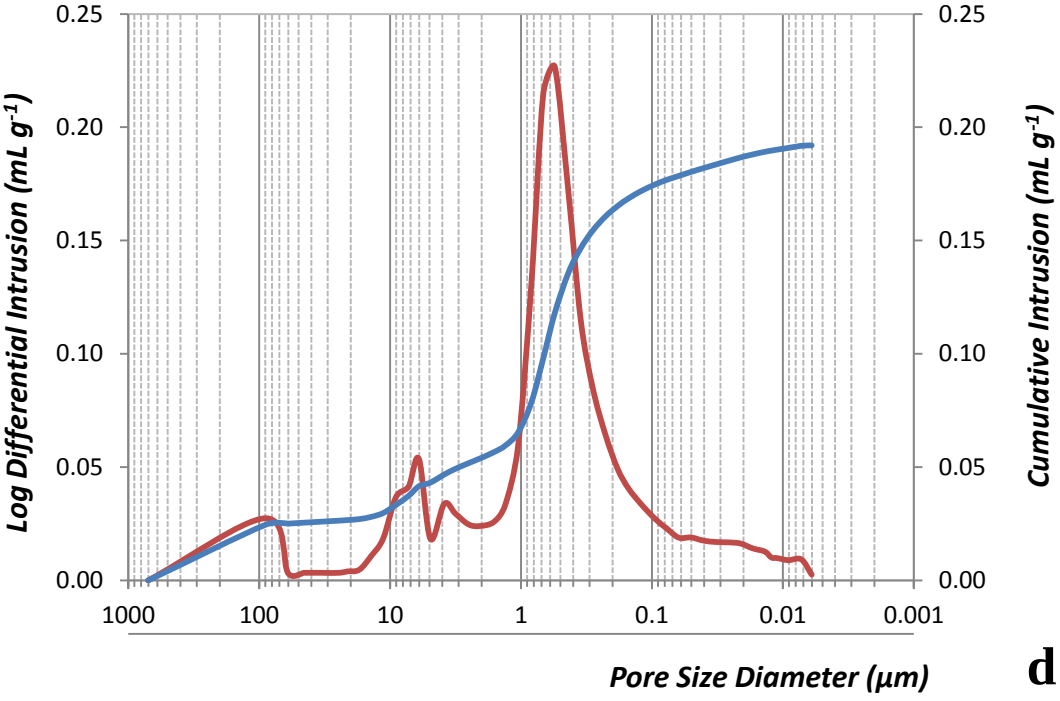
0.25
0.20
0.15
0.10
0.05
0.00
1000
100
10
1
0.1
0.01
0.001
Log Differential Intrusion (mL g-1)
Cumulative Intrusion (mL g-1)
Pore Size Diameter (µm)

d

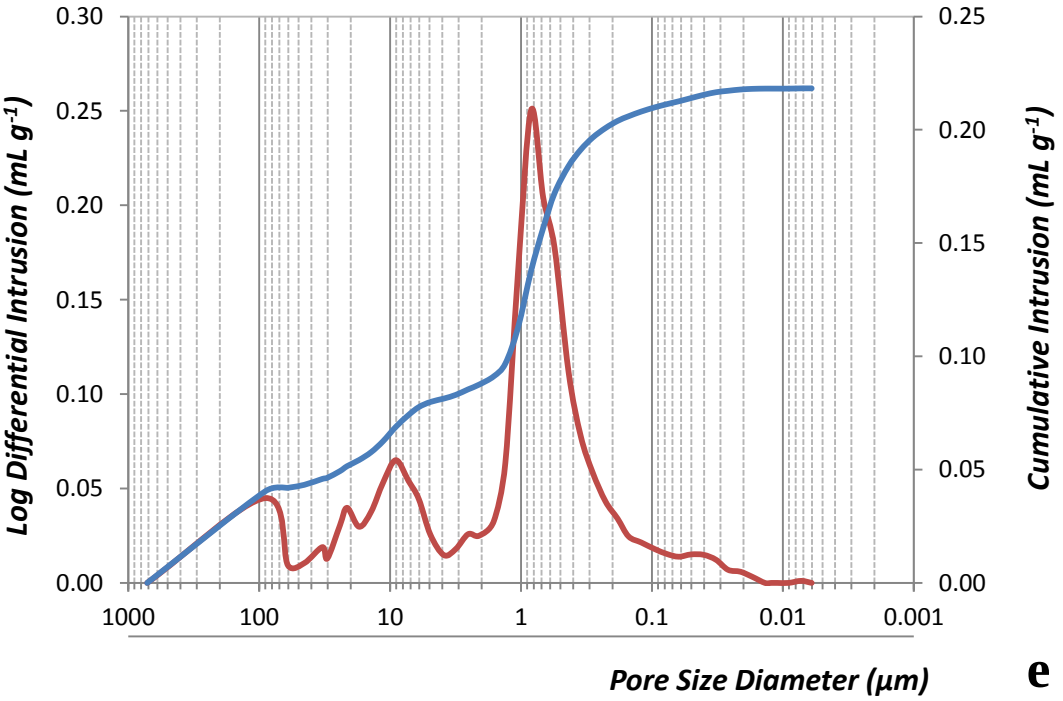

Figure 3. Differential pore size distribution and Hg-intrusion cumulative curves obtained by MIP of MS2 samples subjected to different water removal procedures: solvent-exchange drying method (a), freeze-drying (b), vacuum drying (c), oven drying at 60ºC (d) and oven drying at 105ºC (e), after 28 curing days.

Figure 4 rv

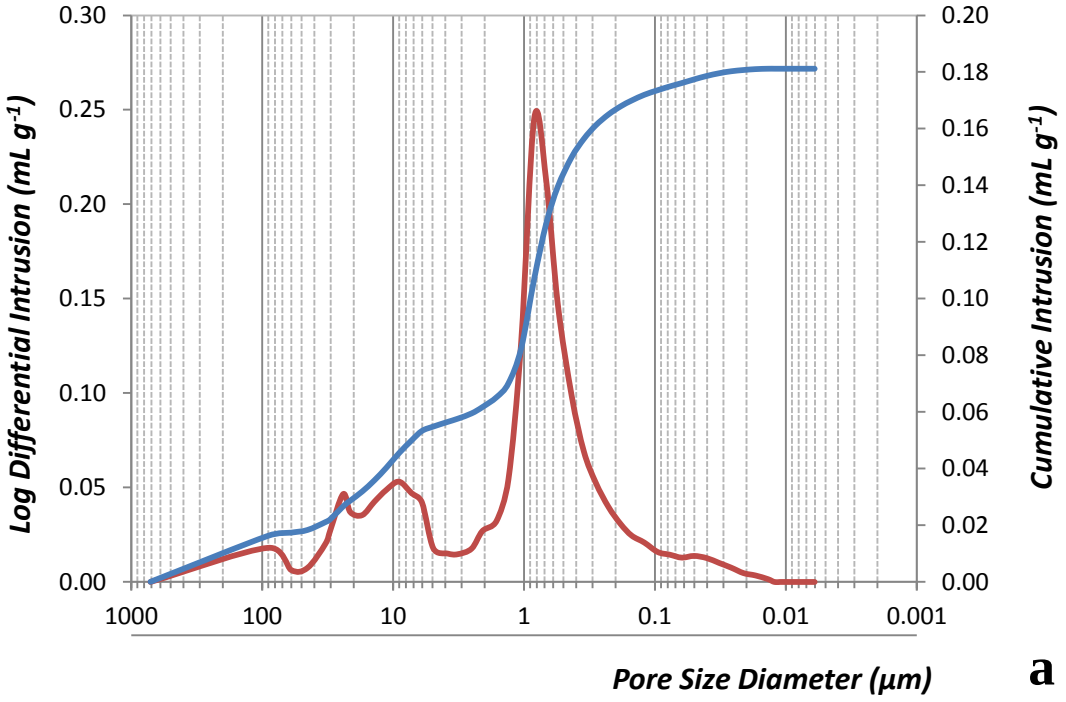

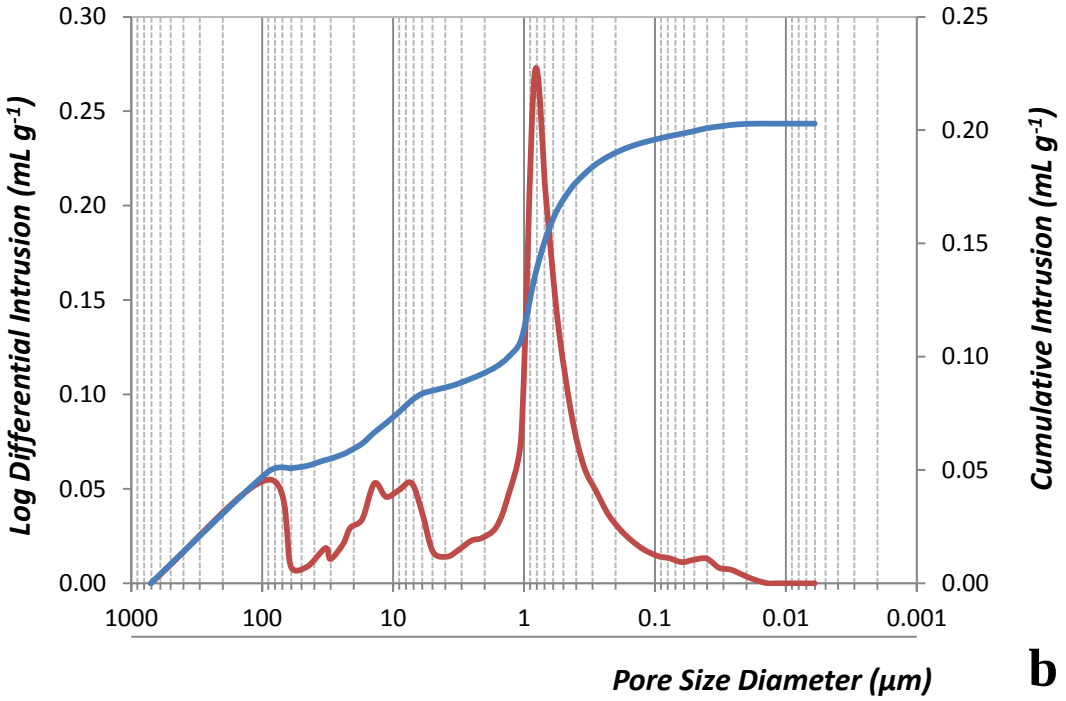

Figure 4. Differential pore size distribution and Hg-intrusion cumulative curves obtained by MIP of MS3 samples subjected to freeze-drying (a) and vacuum drying (b), after 28 curing days.

Figure 5 rv

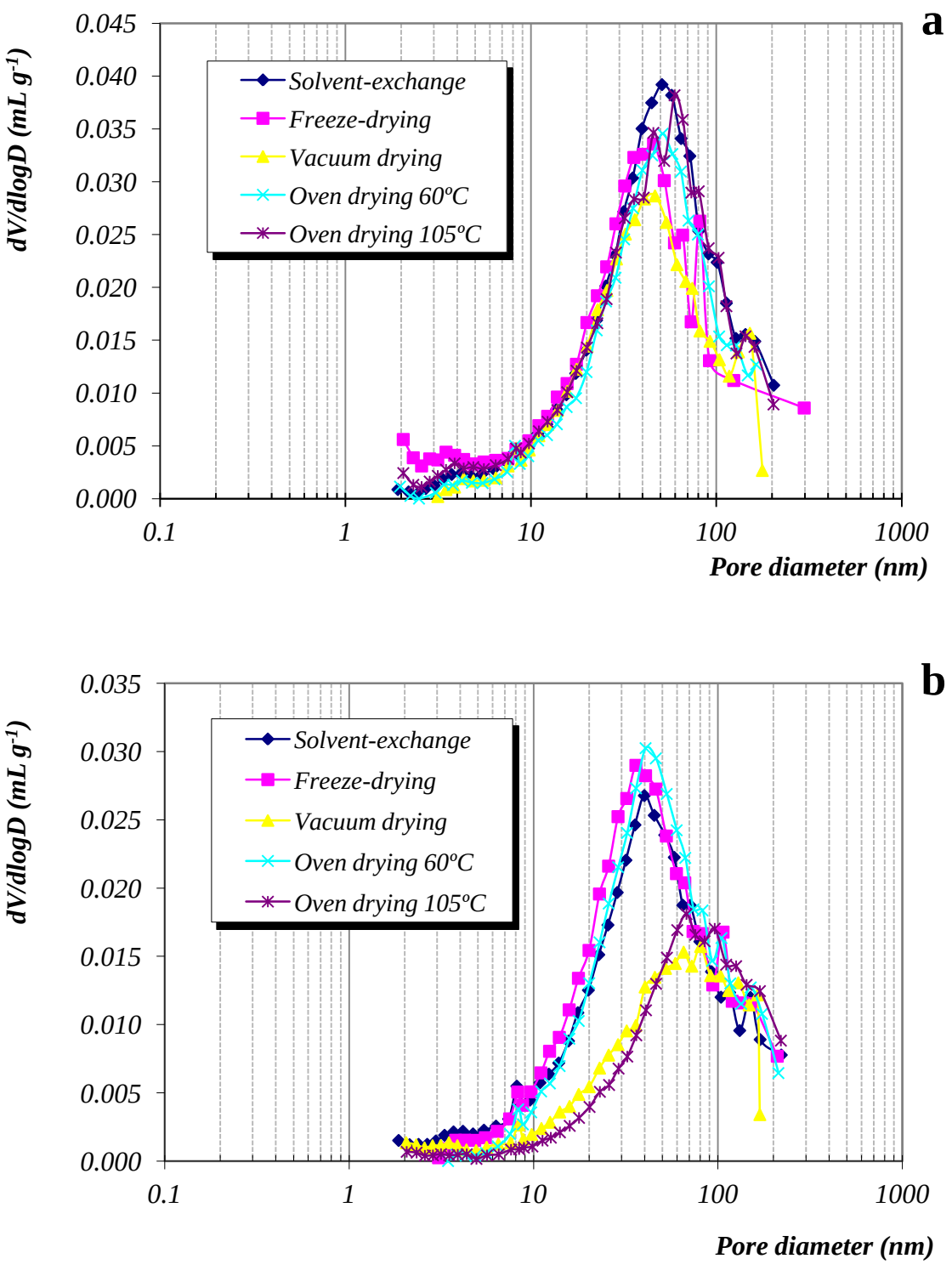
a
dV/dlogD (mL g-1)
0.045
0.040
0.035
0.030
0.025
0.020
0.015
0.010
0.005
0.000
Solvent-exchange
Freeze-drying
Vacuum drying
Oven drying 60ºC
Oven drying 105ºC
0.1
1
10
100
1000
Pore diameter (nm)
b
dV/dlogD (mL g-1)
0.035
0.030
0.025
0.020
0.015
0.010
0.005
0.000
Solvent-exchange
Freeze-drying
Vacuum drying
Oven drying 60ºC
Oven drying 105ºC
0.1
1
10
100
1000
Pore diameter (nm)

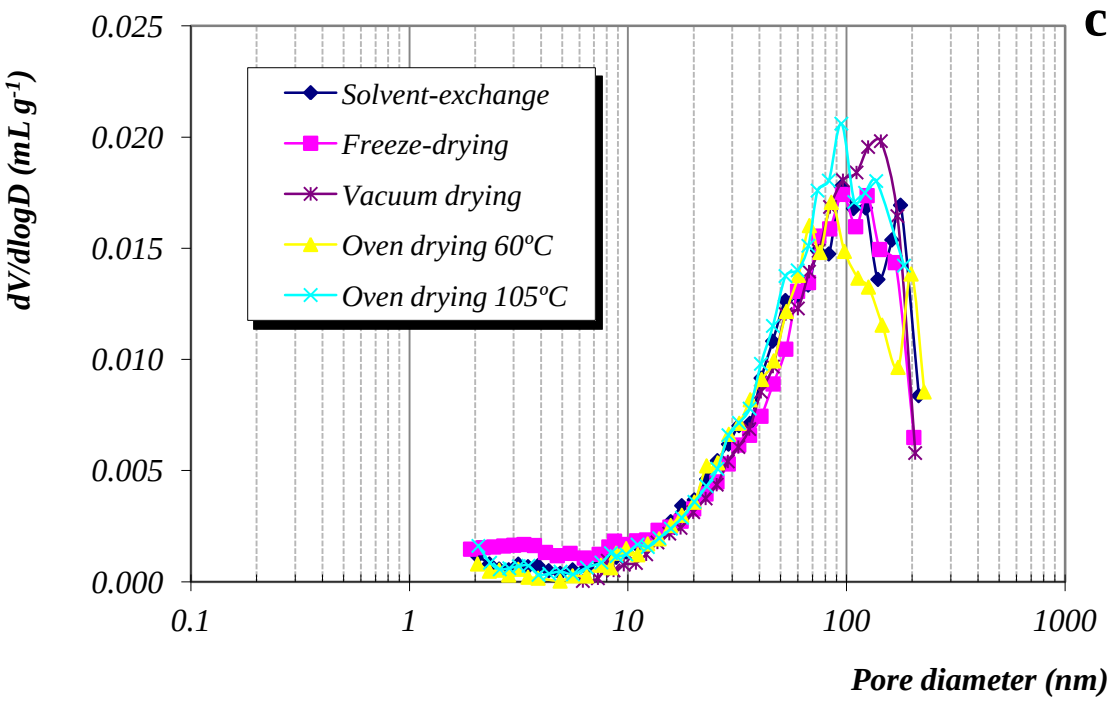

Figure 5. Pore size distribution at the mesopore range obtained by the BJH method for MS1 specimens subjected to the five different water removal procedures after: a) 7 curing days; b) 28 curing days; and c) 91 curing days.

Figure 6 rv

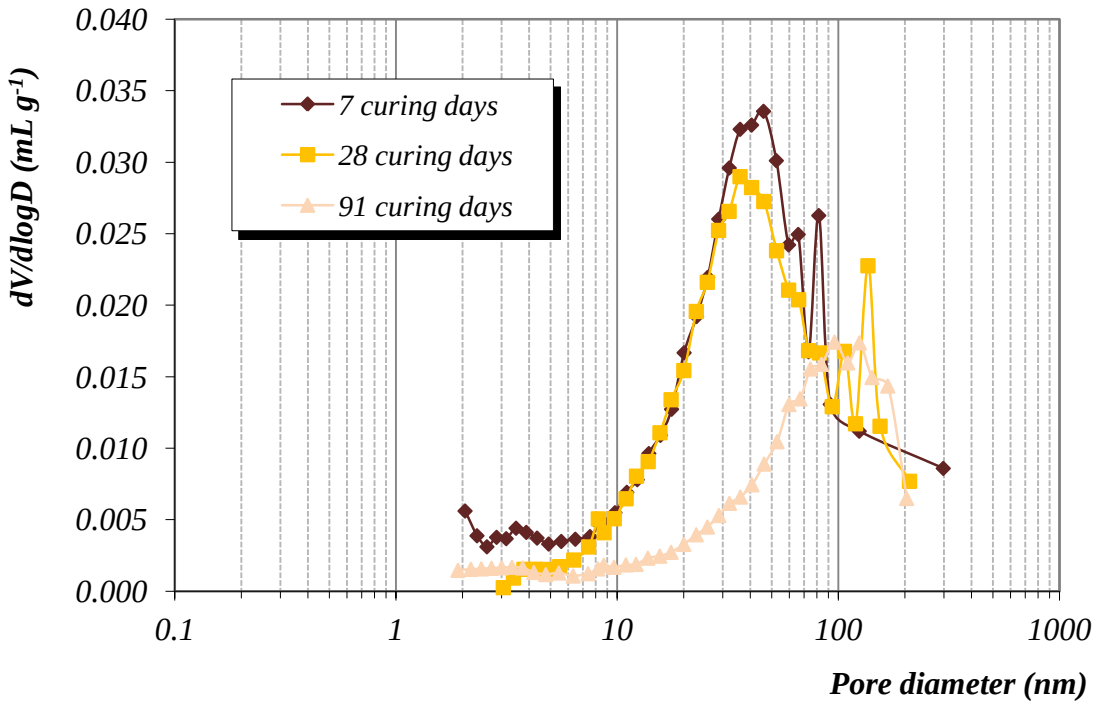

Figure 6. Comparative pore size distribution curves (mesopore range, BJH method) for freeze-dried MS1 samples after different (7, 28 and 91) curing days.

Figure 7 rv

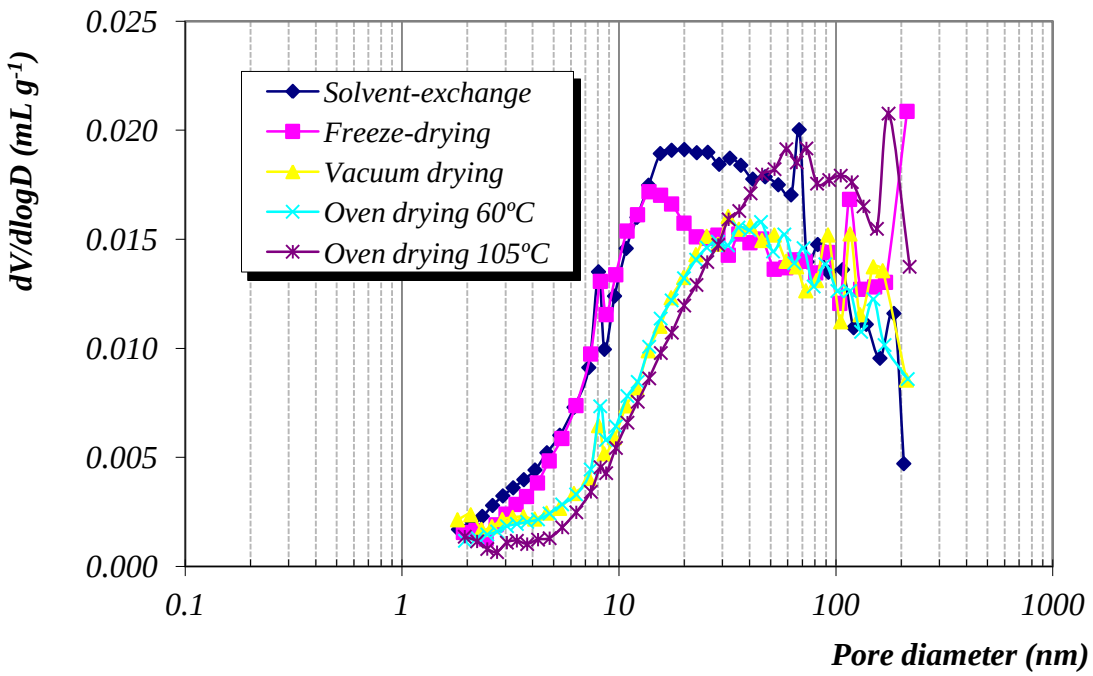

Figure 7. Pore size distribution graphs at the mesopore range obtained by the BJH method for MS2 specimens subjected to the five different water removal procedures after 7 curing days.

Figure 8 rv

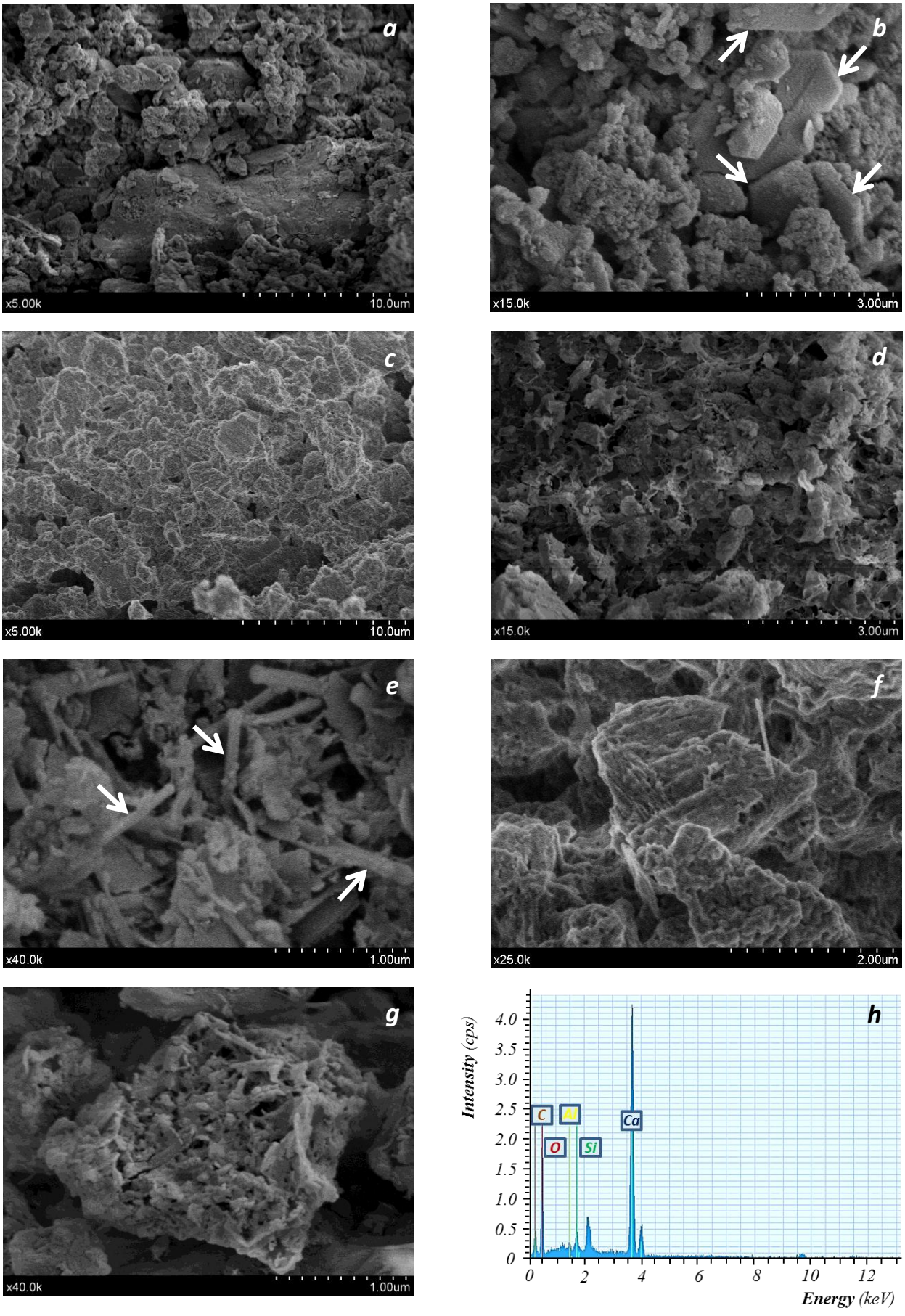
a
x5.00k
10.0um
b
x15.0k
3.00um
c
x5.00k
10.0um
d
x15.0k
3.00um
e
x40.0k
1.00um
f
x25.0k
2.00um
g
x40.0k
1.00um
h
Intensity (cps)
4.0
3.5
3.0
2.5
2.0
1.5
1.0
0.5
0
C
Al
Ca
O
Si
0
2
4
6
8
10
12
Energy (keV)

Figure 8. SEM micrographs of 91-days old specimens of: a) MS1 sample, showing a largely porous matrix of scaleno-rhombohedral calcite crystals; b) detail of MS1 sample depicting, besides calcite crystals, hexagonal plate-like portlandite crystals marked by arrows; c) MS2 sample showing a more compact binding matrix in comparison with MS1 sample in (a); d) detail of honeycomb-shaped C-S-H compounds in a MS2 sample; e) MS2 specimen in which C-S-H fibers can be observed (white arrows); f) detail of a MS2 sample showing a nanosized porosity; g) MS2 specimen showing, in the center of the micrograph, an agglomeration of C-S-H. Chemical composition of this agglomerate yielded mainly Ca, Si and O (EDS analysis) in h).

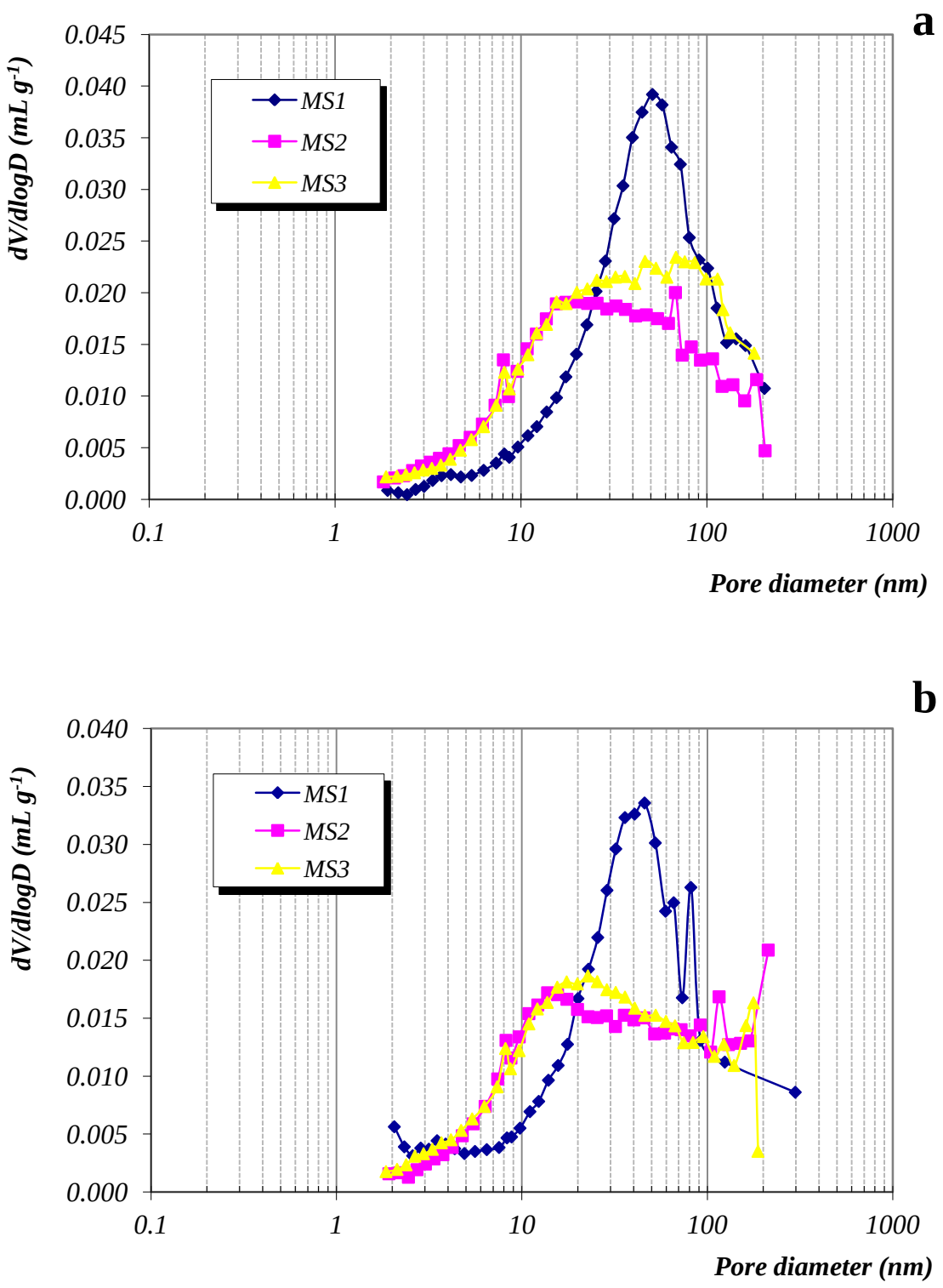

Figure 9. Comparative pore size distribution curves (BJH method) for 7-days old MS1, MS2 and MS3 samples: (a) dried by solvent-exchange and (b) freeze-dried.

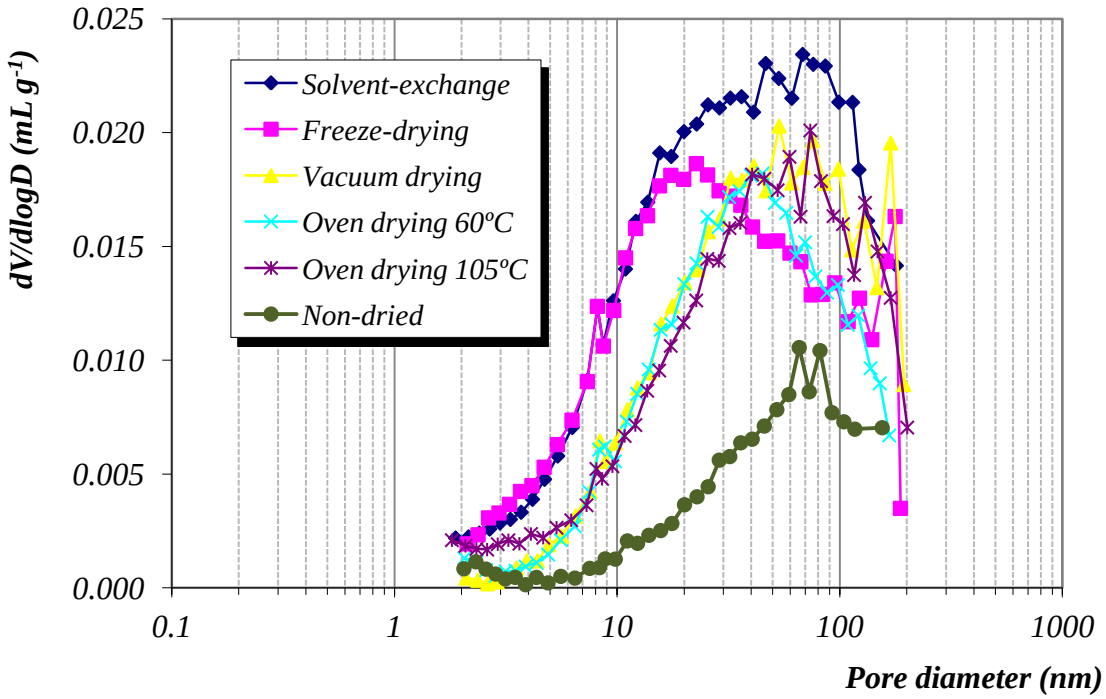

Figure 10. Mesopore PSD of 7-days old MS3 samples subjected to the five different drying methods. PSD of a non-dried sample is also shown for comparison purposes.